Journal of The Electrochemical Society, **149** (12) B551-B559 (2002)
0013-4651/2002/149(12)/B551/9/$7.00 © The Electrochemical Society, Inc.

Thermodynamic Analysis of Alumina Refractory Corrosion by Sodium or Potassium Hydroxide in Glass Melting Furnaces

Karl E. Spear[a,*] and Mark D. Allendorf[b,,z]**

[a]*Department of Materials Science and Engineering, The Pennsylvania State University, University Park, Pennsylvania 16802, USA*
[b]*Sandia National Laboratories, Combustion Research Facility, Livermore, California 94551-0969, USA*

In this paper the high-temperature corrosion of Al_2O_3 refractories by MOH(g) (M = Na, K) found in the combustion atmospheres of typical air- and oxygen-fired glass-melting furnaces is examined using thermodynamic equilibrium calculations. These hydroxide species are considered to be the primary reactive alkali species since their partial pressures are significantly larger than those of M(g), the next most abundant gas-phase alkali-containing species expected in typical furnace atmospheres. Thermochemical simulations show that corrosion of α-alumina by NaOH(g) at typical furnace $p_{NaOH(g)}$ of around 200 ppm under oxy/fuel-fired conditions is unlikely as long as the refractory temperature exceeds 1564 K. For KOH(g) at 200 ppm, the temperature of the refractory must exceed 1515 K to avoid corrosion. Under air-fired conditions, $p_{NaOH(g)}$ is considerably lower (40-80 ppm); at 50 ppm, corrosion is thermodynamically unfavorable at temperatures above 1504 K. For KOH(g) at furnace levels of ~50 ppm, temperatures must be above 1458 K. The paper also presents a re-evaluation of the thermodynamic and phase equilibrium properties of the Na_2O-Al_2O_3 and K_2O-Al_2O_3 binary systems to develop accurate and self-consistent thermodynamic data. The data for MAl_9O_{14} (β-alumina) and $M_2Al_{12}O_{19}$ (β″-alumina) are particularly critical since these phases are likely products of the corrosion of alumina refractories by MOH vapors in glass melting furnaces.
© 2002 The Electrochemical Society. [DOI: 10.1149/1.1516773] All rights reserved.

Manuscript submitted March 1, 2002; revised manuscript received May 24, 2002. Available electronically October 24, 2002.

The corrosion of refractory materials used to line the ceiling or crown of combustion-heated glass-melting furnaces is exacerbated by the introduction of oxy/fuel melting technology in which air is replaced by oxygen as the oxidizer. The concentration of alkali hydroxides (NaOH and/or KOH produced by reaction of combustion-generated water vapor with alkaline oxides in the glass melt) in these furnaces is a factor of two to four times higher than in air-fired furnaces, due to the higher water-vapor concentration that results from removing nitrogen from the combustion gases. This can lead to unusually high corrosion rates for low-density silica refractories, which are often used in air-fired furnaces.[1] Anecdotal reports indicate that reductions in silica crown lifetimes by as much as a factor of two can occur due to corrosion of the refractory. As a result, there is great interest in understanding the mechanisms for this enhanced corrosion and for using this information to design new, more effective refractories.

Alumina-based ceramics, such as bonded and fused cast aluminas [α-alumina (Al_2O_3), β-alumina (a measured experimental composition of $NaAl_9O_{14}$),[2] and a mixture of α-alumina and β-alumina, which we refer to as α-alumina/β-alumina], fused cast alumina-zirconia-silica (AZS), and fused mullite ($Al_6Si_2O_{13}$) provide alternatives to silica refractories. These materials are also subject to varying degrees of corrosion in oxy/fuel environments, however. While silica refractories react with alkali vapors to form low-melting sodium- or potassium-silicate glassy liquids that can drip from the crown into the molten glass,[3] mixing of these corrosion products with the glass melt is not always a problem since the chemical compositions of the two liquids are similar. In the case of alumina-containing refractories, however, formation of corrosion products that can drip, run, or spall into the glass melt can lead to defects in the final product.[4] Thus, there is a need to develop an understanding of the processes leading to corrosion of these alternative refractories in oxy/fuel furnaces to determine how furnace designs and/or operating conditions can be adjusted to reduce or eliminate corrosion. Thermodynamic calculations (*i.e.*, predictions of chemical compositions based on minimization of the Gibbs free energy) can play a useful role by identifying energetically stable species and predicting the extent of corrosion and formation of products. The high temperatures at crown surfaces (>1850 K in some locations)[5] and long reaction times of months to years indicate that equilibrium should be a valid approximation to the chemistry.

To perform such calculations, however, it is critical to develop internally consistent thermodynamic properties for all phases in these systems, including liquids, since liquid corrosion products can be a factor in refractory corrosion in glass furnaces. With a complete set of data for each system, equilibrium calculations can then be used to assess the potential importance of all possible product phases in the corrosion process.

Corrosion of alumina by sodium has been of interest for some time due to its use in low-pressure sodium discharge lamp envelopes,[6,7] in composites,[8,9] and structural ceramics. Using various qualitative and semiquantitative methods, the stability of alumina-containing refractories in glass-melting environments has been evaluated.[4] In general, β-alumina and α-alumina/β-alumina perform better than most other refractories in high-alkali environments. β-alumina is also of interest as a sodium-ion-conducting solid electrolyte, and thus its thermodynamic stability is of importance to this application as well.[10] Equilibrium calculations used to predict the stability of alumina refractories are reported in two studies;[4,11] however, it is unclear if internally consistent thermodynamic data were used. The results suggest that both α-alumina and α-alumina/β-alumina should be stable under typical oxy-fuel melting conditions and that alumina is more resistant to alkali attack than silica.

Earlier reports of thermodynamic properties (such as heats of formation, entropies, heat capacities, heats of transition, and activities) and phase diagrams for both the Na_2O-Al_2O_3 and K_2O-Al_2O_3 systems are summarized and critically evaluated by Eriksson *et al.*[12] The Na_2O-Al_2O_3 phase equilibria data were also thoroughly evaluated by Roth.[13] Thermodynamic data, primarily heats of formation and M_2O activities, for crystalline phases in the M_2O-Al_2O_3 (M = Na, K) systems are reported by several investigators. Specific reports and reviews are given for Na_2O activity measurements in α-β alumina two-phase compositions,[2,10,14-16] and for K_2O activity measurements in similar composition regions.[14,17,18]

The optimized phase diagrams published by Eriksson *et al.*[12] for the Na_2O- and K_2O-Al_2O_3 systems do not extend to M_2O mole fractions less than 0.5, but these authors have generated thermodynamic information for the liquid phases in the alumina-rich part of

* Electrochemical Society Fellow.
** Electrochemical Society Active Member.
z E-mail: mdallen@sandia.gov

the diagrams. These compositions include the sodium- or potassium-containing liquid products that can form when either pure α-alumina or β-alumina reacts with alkali vapors. Eriksson *et al.*[12] used quasi-chemical model parameters to represent nonideal interactions in these liquid phases. However, these parameters are not easily adapted to the modified associate species model we are using for liquid solution phases.[3]

In this paper, we present a re-evaluation of the thermodynamic properties of the M_2O-Al_2O_3 binary systems (M = Na or K) to determine self-consistent sets of accurate thermodynamic information. The beta-aluminas, MAl_9O_{14} (β-alumina) and $M_2Al_{12}O_{19}$ (β″-alumina), are likely products of the corrosion of α-alumina by MOH vapors present in glass furnaces. Conditions required for reactions of MOH(g) with Al_2O_3 refractories in representative air- and oxygen-fired combustion atmospheres were determined. Our focus is on reactions involving MOH(g) since the hydroxide is the primary alkali-containing gaseous species; M(g) pressures are significantly smaller than the MOH(g) pressures in these furnace atmospheres. In addition to discussing the temperature dependence of MOH(g) and M(g) concentrations, we present graphs for both alkali-containing systems, from which a critical temperature for corrosion can be determined for any MOH(g) partial pressure in the furnace atmosphere between 0 and 1000 ppm. Due to the high liquidus temperatures of >2150 K in the α-β regions of both the Na_2O-Al_2O_3 and K_2O-Al_2O_3 systems, the formation of low-viscosity liquids is unlikely under conditions typical of most air- and oxy-fuel glass melting furnaces.

Equilibrium Modeling Approach

To model alumina corrosion at equilibrium, one needs to know the partial pressure of H_2O(g) (p_{H_2O}), the activities of M_2O (a_{M_2O}) as a function of temperature and composition, and the temperature-dependent equilibrium constants K_{eq} for all phase regions in the M_2O-Al_2O_3 systems. Thus, thermodynamic data such as heats of formation, entropies, heat capacities, heats of transition, and activities are needed for all gaseous and condensed species in the systems, including the crystalline and liquid phases that may be formed by the corrosion process. The required information for most gas-phase species was obtained from the assessed SGTE database.[19] However, the $\Delta H^o_{f,298}$ value for NaOH(g) in this database (−185.649 kJ/mol) is quite different from that found in the *JANAF Thermochemical Tables* (−197.757 kJ/mol).[20] The corresponding values of the entropy (S^o_{298}) from these two sources are quite similar, however, being 228.589 and 228.443 J/mol K, respectively. The $\Delta H^o_{f,298}$ and S^o_{298} values for solid NaOH(s) from the two sources are also essentially the same. Thus, the 12 kJ/mol difference in the $\Delta H^o_{f,298}$ values for NaOH(g) appears to be the only major uncertainty in the sodium hydroxide data used in our calculations. In the calculations described here, we chose to use the JANAF value for $\Delta H^o_{f,298}$(NaOH,g), for reasons that are discussed in detail in a previous communication.[3]

Tabulated thermodynamic properties for liquid-phase corrosion products are lacking, so these values were determined along with an assessment and optimization of the values for crystalline phases in both the Na_2O-Al_2O_3 and K_2O-Al_2O_3 binary systems. The computer program ChemSage™[21] was our primary tool for developing an assessed, internally consistent thermodynamic database for these two M_2O-Al_2O_3 systems and for performing subsequent calculations of the high-temperature corrosion reactions between their MOH(g) vapors and Al_2O_3(s). The following paragraphs describe our analysis of available thermochemical information for these systems and our choices for the values used in the equilibrium calculations described later in this paper.

In developing self-consistent sets of thermodynamic properties for each system, we modeled the thermodynamic stabilities of M_2O-containing liquid-oxide solutions using a modified associate species approach described previously.[22] The negative free-energy terms caused by nonideal mixing of end-member liquid components in a system are contained in the formation energies of the liquid associate species in this model. For the two systems examined in this paper, only ideal mixing of associate liquid species was needed to model the two respective liquid phases; no nonideal solution parameters were needed. In both M_2O-Al_2O_3 binary systems, we modeled the liquid by using four liquid associate species of M_2O(l), $MAlO_2$(l), (1/3)$M_2Al_4O_7$(l), and Al_2O_3(l). To provide equal weighting of liquid species, the composition of each liquid associate has a total of two non-oxygen atoms in its formula. While these four liquid species may not exist as chemical entities that can be isolated and characterized, their formation energies and the ideal solutions comprised of them accurately represent the negative interaction energies that occur between M_2O and Al_2O_3 in these two alkali liquid oxide solutions. The ternary Na_2O-K_2O-Al_2O_3 is not examined in this paper.

Table I. Typical input conditions for equilibrium calculations. *P*(total) = 1 bar, *T* = 1173-2373 K (900-2100°C).

	$n(CH_4)$[a]	$n(O_2)$[a]	$n(N_2)$[a]	$n(M_2O)$[a,c]	a (refractory)[b]
Calculation of p_{H_2O}					
Air-fired	1.00	2.05	8.2	-	-
Oxygen-fired	1.00	2.05	-	-	-
Corrosion predictions					
Air-fired	1.00	2.05	8.2	0.1	1.0 (α)
Oxygen-fired	1.00	2.05	-	0.1	1.0 (α)
Air-fired	1.00	2.05	8.2	0.1	1.0 (β)
Oxygen-fired	1.00	2.05	-	0.1	1.0 (β)

[a] Moles.
[b] Activity of either α-Al_2O_3 or β-alumina was fixed at unity.
[c] M = Na or K.

The thermodynamic data for the binary M_2O-Al_2O_3 systems were assessed and optimized by performing a manual thermodynamic fitting of the binary equilibrium phase diagram for the two alkali-containing systems (see Ref. 12, 13, 23, and the references cited therein for the latest phase diagram data). Results were also compared with published thermodynamic activity values and assessments for the systems (see Ref. 2, 10, 12, 14-20). This procedure provides a means of testing and generating a set of self-consistent thermodynamic information for the systems, including data for the oxide liquid phases.[3,22] Using the resulting thermodynamic properties, we calculated the equilibrium compositions of the two systems using input conditions typical of air- and oxy-fuel glass melting furnaces. Input parameters used to perform the equilibrium calculations are given in Table I. These conditions were chosen so that either crystalline α- or β-alumina is always present, as indicated in the last column of Table I, which ensures the existence of the chosen crystalline alumina refractory at equilibrium. All calculations were performed at a pressure of 1 bar. The major species included in the various calculations are given in Table II, which also includes the source for the thermodynamic data in each case. Table III gives thermodynamic data for important species used in the calculations in the Na_2O-Al_2O_3 and K_2O-Al_2O_3 systems.

Results

Na_2O-Al_2O_3 phase diagram and Na_2O activities.—The calculated phase diagram resulting from our assessed dataset is shown in Fig. 1a for the Na_2O-Al_2O_3 system. This diagram is generally in good agreement with the assessed diagrams given by Roth[13] and Eriksson *et al.*[12] except for a slight difference in the melting temperature for $NaAl_9O_{14}$, for which there is little experimental information. The thermodynamic stability of the liquid is changed very little by the differences. In Fig. 1b, we also compare our calculated Na_2O activities for the α-Al_2O_3-β-$NaAl_9O_{14}$ two-phase region with the more recent values reported in the literature (see Ref. 2, 10,

Table II. Major species used in calculations and sources of thermodynamic data.

Gas-phase[a]				
N_2	H_2O	CH_4	O_2	NO
H_2	OH	CO_2	NO_2	N_2O
H	CO	HCN	NH_3	
Na	NaOH[b]	K	KOH	
Liquid phase[c]				
$Na_2O(l)$	$NaAlO_2(l)$	$(1/3)Na_2Al_4O_7(l)$	$Al_2O_3(l)$	
$K_2O(l)$	$KAlO_2(l)$	$(1/3)K_2Al_4O_7(l)$		
Solid Phase[d]				
Na_2O	$NaAlO_2$	$Na_2Al_{12}O_{19}(\beta'')$	$NaAl_9O_{14}(\beta)$	$Al_2O_3(\alpha)$
K_2O	$KAlO_2$	$K_2Al_{12}O_{19}(\beta'')$	$KAl_9O_{14}(\beta)$	
Na_2CO_3	K_2CO_3			

[a] A total of 75 gaseous species were initially used in these calculations. The major source of these data was SGTE (Ref. 19) except as noted.
[b] JANAF (Ref. 20).
[c] The set of liquid associate species was developed in the current studies.
[d] Additional fixed-composition nitride and carbide phases were initially used in these calculations, but were always at very low activities. The source of liquid- and solid-phase thermodynamic data is our current assessment of the type described in Ref. 22, using initial thermodynamics values from the literature (Ref. 2, 10, 12, 14-20).

14, 15). Nafe,[10] Petric and Chatillon,[15] and Jacobs *et al.*[2] also show graphs including other reported activity values along with their own respective measurements. Except for the high-temperature mass spectrometric vapor pressure measurements of Petric and Chatillon, all other activity measurements were made using lower temperature solid-state electrolyte galvanic cells.

K_2O-Al_2O_3 phase diagram and K_2O activities.—Our calculated phase diagram for the K_2O-Al_2O_3 system is shown in Fig. 2a, and is also in good agreement with the assessed diagram given by Eriksson *et al.*,[12] except for a slight difference in the melting temperature of KAl_9O_{14}, for which there is little experimental information. The thermodynamic stability of the liquid is changed very little by the differences. As discussed by Eriksson *et al.*,[12] the very existence of the β''-alumina ($K_2Al_{12}O_{19}$) is uncertain, let alone its peritectoid decomposition temperature. Eriksson *et al.*[12] show the β-phase melting by a peritectic reaction at 1920°C to give α-alumina and liquid [mole fraction $X(Al_2O_3) = 0.75$]. In contrast, our calculated diagram has a congruently melting β-phase at 1989°C and an α-alumina/β-alumina eutectic at 1984°C, as shown in Fig. 2a.

We also compared our calculated K_2O activities for the α-Al_2O_3-β-KAl_9O_{14} two-phase region with those reported in the literature (see Ref. 14, 17, 18); the results are shown in Fig. 2b. Possible reasons for the high values of Kumar and Kay[14] have been thoroughly discussed by Kale and Jacob.[17] The reported experimental studies in this system all involved solid-state electrochemical cells.

The phase diagrams in Fig. 1a and 2a clearly show why alumina-based ceramics are more resistant to corrosion by NaOH or KOH than silica.[3] In contrast with silica corrosion, the formation of liquid-phase products relatively rich in M_2O can only occur at very high temperatures in the M_2O-Al_2O_3 systems. Such products are not present until the temperature reaches 1857 K (1584°C) for the sodium case, and 2185 K (1912°C) for the potassium case, where β-alumina reacts to form a liquid. In the Na_2O-SiO_2 system, liquids can form at temperatures as low as 1090 K.[3] Pure α-alumina in contact with MOH(g) cannot form a liquid until the temperature reaches 2158 K for M = Na, or 2257 K for M = K.

Corrosion modeling approach.—We now discuss the chemical reactions involved in the corrosion of α- and β-alumina by NaOH and KOH. Equilibrium calculations by ourselves and others[3,24,25]

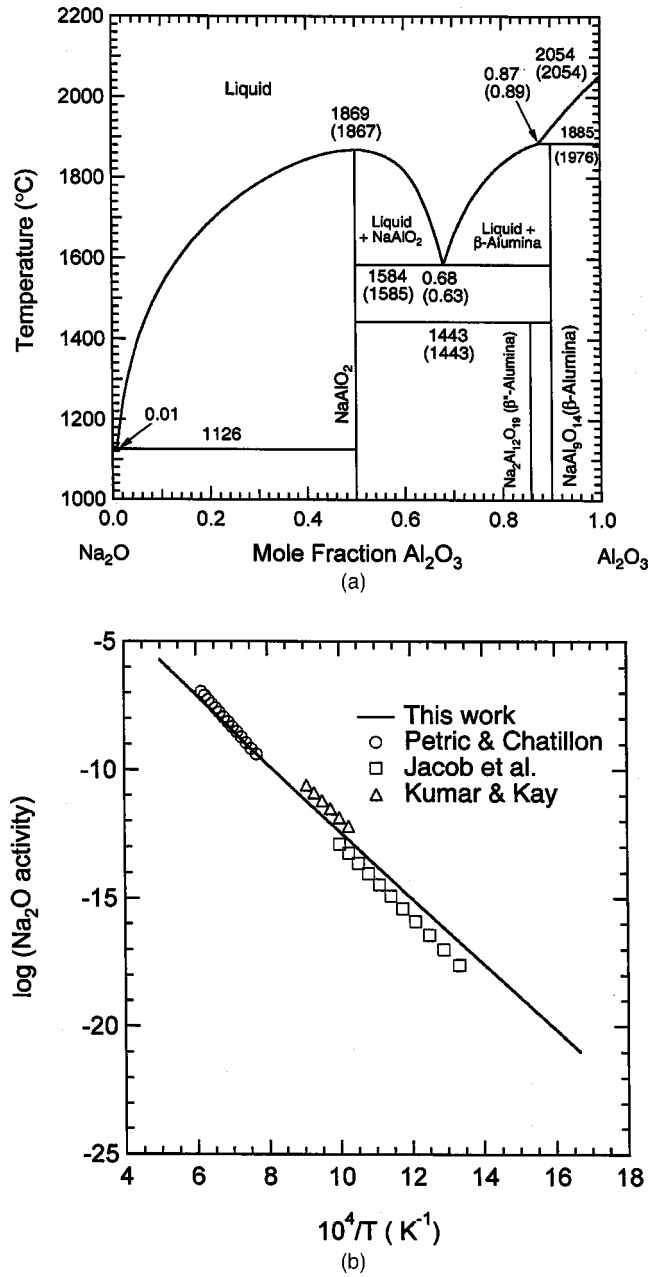

Figure 1. (a) Calculated phase diagram for the Na_2O-Al_2O_3 system. Note that temperatures are given in °C for ease of comparison with published phase diagrams; most temperatures in this article are given in K. Current temperatures are shown, along with previously reported values in parentheses; Ref. 12, Eriksson *et al.* (b) Calculated $\ln a(Na_2O)$ *vs.* $10^4/T$ in the α-alumina/β-alumina two-phase region in the Na_2O-Al_2O_3 system.

show that NaOH(g) is the most abundant sodium-containing gas when the combustion atmosphere equilibrates with sodium-containing glass melts. This is also true for KOH(g) in glass melts containing potassium. Therefore, we assume that NaOH(g) is the key sodium-containing species participating in the corrosion of alumina, and that KOH(g) is the key potassium-containing species involved. The formation of these hydroxides can be described by the following generic chemical reaction, where M = Na or K

$$M_2O(\text{in glass melt}) + H_2O(\text{g, combustion gas}) \rightleftarrows 2MOH(g) \quad [1]$$

Table III. Thermodynamic data for important species in Na_2O-Al_2O_3 and K_2O-Al_2O_3 systems.

Species	$\Delta H^o_{f,298}$ (J/mol)	S^o_{298} (J/mol-K)	T (K)	$Cp = a + bT + cT^2 + d/T^2$ (J/mol-K) a	$b10^3$	$c10^6$	$d10^{-5}$
Gases							
Na	107,500	153.716	2700	21.025	−0.384	0.143	−0.134
			5500	13.002	1.375	0.199	208.714
NaOH[a]	−197,322	228.443	1500	51.971	2.281	0.778	−3.848
			6000	58.196	1.315	−0.115	−66.087
K	89,000	160.339	2100	21.136	−0.653	0.293	−0.172
			4500	16.475	−0.366	0.709	98.005
KOH	−232,630	236.376	1200	53.038	−0.004	2.094	−4.168
			3200	52.639	4.546	−0.614	−20.879
Liquid associates							
$Na_2O(l)$	−370,284	108.988	1023	55.480	70.210	−30.540	−4.140
	$\Delta H^o_{trans}(1023\ K) = 1{,}757$		1243	82.563	12.350	0	0
	$\Delta H^o_{trans}(1243\ K) = 11{,}924$		1405	82.563	12.350	0	0
			3500	104.600	0	0	0
$NaAlO_2(l)$	−1,000,000	107.000	1000	86.485	40.295	−15.270	−20.625
			1923	100.027	11.365	0	−18.555
			3000	148.532	0	0	0
$Na_2Al_4O_7(1/3)$	−1,234,000	95.000	1000	96.820	30.323	−10.180	−26.120
			1923	105.848	11.037	0	−24.740
			3000	163.176	0	0	0
$K_2O(l)$	−327,300	129.958	1013	75.947	17.146	0	−5.916
			3000	100.000	0	0	0
$KAlO_2(l)$	−1,040,000	114.250	1000	96.719	13.763	0	−15.597
			2533	111.045	5.190	0	−18.555
			3000	148.532	0	0	0
$K_2Al_4O_7(1/3)$	−1,210,000	102.000	1000	103.642	12.635	0	−22.770
			2533	108.745	6.920	0	−24.740
			3000	161.643	0	0	0
$Al_2O_3(l)$	−1,564,604	98.679	2327	117.490	10.380	0	−37.110
			4000	192.464	0	0	0
Crystalline solids							
Na_2O	−417,982	75.040	1023	55.480	70.210	−30.540	−4.140
	−417,982[b]	*75.061*[b]					
	$\Delta H^o_{trans}(1023\ K) = 1{,}757$		1243	82.563	12.350	0	0
	$\Delta H^o_{trans}(1243\ K) = 11{,}924$		1405	82.563	12.350	0	0
			3500	104.600	0	0	0
$NaAlO_2$	−1,111,000	64.500	1000	86.485	40.295	−15.270	−20.625
	−1,119,572	*65.321*	1923	100.027	11.365	0	−18.555
			3000	148.532	0	0	0
$Na_2Al_{12}O_{19}$	−10,685,000	369.750	1000	760.420	132.490	−30.540	−226.800
	−10,702,896	*358.119*	2000	787.503	74.630	0	−222.660
			3000	1259.384	0	0	0
$NaAl_9O_{14}$	−7,873,000	262.000	1000	556.445	81.800	−15.270	−169.065
	−7,873,369	*258.876*	2273	569.985	52.900	0	−166.995
			3000	918.390	0	0	0
K_2O	−361,700	96.000	1013	75.947	17.146	0	−5.916
	−361,498	*102.006*	3000	100.000	0	0	0
$KAlO_2$	−1,144,000	74.500	1000	96.719	13.763	0	−15.597
	−1,145,224	*81.159*	2533	108.745	5.190	0	−18.555
			3000	146.232	0	0	0
$K_2Al_{12}O_{19}$	−10,740,000	386.000	1000	780.887	79.426	0	−216.744
	−10,788,495	*374.908*	2200	804.940	62.280	0	−222.660
			3000	1254.784	0	0	0
KAl_9O_{14}	−7,900,000	268.000	1000	566.679	55.283	0	−164.037
	−7,916,168	*267.271*	2193	578.705	46.710	0	−166.995
			3000	916.088	0	0	0
Al_2O_3	−1,675,692	50.940	2327	117.490	10.380	0	−37.110
	−1,675,700	*50.820*	4000	192.464	0	0	0

[a] Data from Ref. 20; see text for discussion of uncertainties in NaOH(g) data.
[b] Values for $\Delta H^o_{f,298}$ and S^o_{298} in italics are from Eriksson *et al.*[19]

At the surface of the refractory, the MOH can then react to form several products, as is evident from the phase diagrams in Fig. 1a and 2a. The activity of condensed M_2O in the glass, $a(M_2O)$, is determined by the temperature and composition of the glass melt. The p_{H_2O} value expected in the combustion atmosphere of an air-fired furnace is fixed by the fuel/air ratio at ~0.18 bar (in the calculations reported here, p_{H_2O} was calculated from the fuel/oxidizer ratios given in Table I). Anecdotal reports indicate that the resulting NaOH(g) pressure is $\sim 4 \times 10^{-5}$ to 8×10^{-5} bar (40-80 ppm) for typical soda-lime-silica glass melting. The corresponding values for

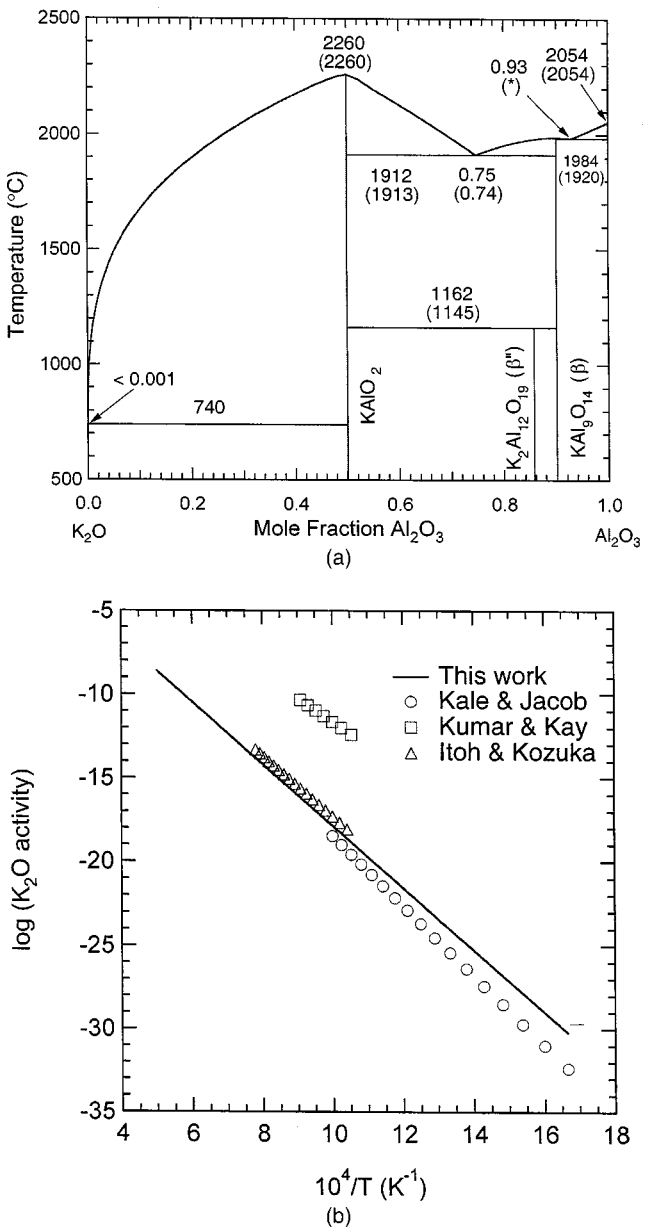

Figure 2. (a) Calculated phase diagram for the K_2O-Al_2O_3 system. The 1 bar gas phase that can occur at temperatures above ~1500°C at the K_2O boundary of this diagram is not shown. Note that temperatures are given in °C for ease of comparison with published phase diagrams; most temperatures in this article are given in K. Current temperatures are shown, along with previously reported values in parentheses; Ref. 12, Eriksson *et al.** For explanation of melting in the α-alumina/β-alumina two-phase region, see Results section of text. (b) Calculated ln $a(K_2O)$ *vs.* $10^4/T$ in the α-alumina/β-alumina two-phase region in the K_2O-Al_2O_3 system.

oxy-fired furnaces are ~0.65 bar for the fixed partial pressure of $H_2O(g)$ and $\sim 1 \times 10^{-4}$ to 2.5×10^{-4} bar (100-250 ppm) for NaOH(g); these results are consistent with NaOH measurements by Walsh *et al.* based on atomic-sodium absorption spectroscopy.[26] For purposes of illustration in the remainder of the paper, we use 50 ppm as a representative p_{NaOH} for air-fired furnaces and 200 ppm for oxy-fired furnaces. We note, however, that NaOH(g) partial pressures are expected to vary from furnace to furnace. Thus, the thermodynamic potential for corrosion in a specific combustion environment can be evaluated from plots of the equilibrium NaOH(g) pressure given below.

For corrosion of alumina by NaOH(g) to occur, the phase diagram in Fig. 1a shows that several reactions are possible. First, if NaOH(g) reacts with α-alumina, crystalline β-alumina can form at $T \leqslant 2158$ K (1885°C; Reaction 2, below). At $T > 2158$ K, the NaOH(g) would react to form an alumina-rich liquid solution (Reaction 3, below)

$T < 2158$ K

$$2NaOH(g) + 9Al_2O_3 \rightleftarrows 2NaAl_9O_{14} + H_2O(g, \text{combustion gas}) \quad [2]$$

$T > 2158$ K

$$2NaOH(g) \rightleftarrows Na_2O(\text{in } Al_2O_3\text{-rich liquid}) + H_2O(g, \text{combustion gas}) \quad [3]$$

Since the equilibrium value of p_{H_2O} in a melting furnace is fixed by the fuel/oxidizer ratio, the p_{NaOH} in equilibrium with both α-alumina refractory and a corrosion product (Reactions 2 or 3) is fixed at one value for a given temperature and partial pressure of water. Similarly, for Reaction 3 under these conditions, the composition of the Al_2O_3-rich liquid corrosion product is also determined. If the combustion atmosphere has a larger p_{NaOH} than the equilibrium value for Reaction 2, then this reaction proceeds to the right and β-alumina ($NaAl_9O_{14}$) can form. Likewise, if the combustion atmosphere has a larger p_{NaOH} than the equilibrium value for Reaction 3, then this reaction proceeds to the right and an Al_2O_3-rich liquid can form.

Second, NaOH(g) can react with β-alumina. At temperatures above 1857 K (1584°C; the eutectic point between $NaAlO_2$ and β-alumina) and Al_2O_3 mole fractions $0.68 < X_{Al_2O_3} < 0.9$, formation of liquid products can occur, with the liquid being in local equilibrium with β-alumina. NaOH(g) can also react with β-alumina to form β″-alumina at $T < 1716$ K (1443°C; Reaction 4), or $NaAlO_2$ at temperatures between 1716 and 1857 K (1443 and 1584°C; Reaction 5).

$$4NaAl_9O_{14} + 2NaOH(g) \rightleftarrows 3Na_2Al_{12}O_{19} + H_2O(g) \quad [4]$$

$$NaAl_9O_{14} + 8NaOH(g) \rightleftarrows 9NaAlO_2 + 4H_2O(g) \quad [5]$$

Similar arguments also hold for the case of potassium in glass melting furnaces. The K_2O-Al_2O_3 phase diagram in Fig. 2a shows that if K_2O reacts with α-alumina, crystalline β-alumina in this system can form at $T \leqslant 2257$ K (1984°C; Reaction 6, below). At $T > 2257$ K, the K_2O would react to form an alumina-rich liquid solution (Reaction 7, below)

$T < 2257$ K

$$2KOH(g) + 9Al_2O_3 \rightleftarrows 2KAl_9O_{14} + H_2O(g, \text{combustion gas}) \quad [6]$$

$T > 2257$ K

$$2KOH(g) \rightleftarrows K_2O(\text{in } Al_2O_3\text{-rich liquid}) + H_2O(g, \text{combustion gas}) \quad [7]$$

Reactions 6 and 7 have only one equilibrium value for p_{KOH} at a given temperature and partial pressure of water if α-alumina is present at equilibrium. For Reaction 7 under these conditions, the composition of the Al_2O_3-rich liquid is also determined. If the combustion atmosphere has a larger p_{KOH} than the equilibrium value for Reaction 6, then this reaction proceeds to the right and β-alumina can form. Similarly, if the combustion atmosphere has a larger p_{KOH} than the equilibrium value for Reaction 7, then this reaction proceeds to the right and an Al_2O_3-rich liquid can form.

At temperatures above 2185 K (1912°C; the eutectic point between $KAlO_2$ and β-alumina) and $0.75 < X_{Al_2O_3} < 0.9$, liquid formation can also occur with the liquid being in local equilibrium with β-alumina. Finally, KOH(g) can react with β-alumina to form β″-alumina at $T < 1435$ K (1162°C; Reaction 8), or $KAlO_2$ at temperatures between 1435 and 2185 K (Reaction 9)

$$4KAl_9O_{14} + 2KOH(g) \rightleftarrows 3K_2Al_{12}O_{19} + H_2O(g) \quad [8]$$

$$KAl_9O_{14} + 8KOH(g) \rightleftarrows 9KAlO_2 + 4H_2O(g) \quad [9]$$

The MOH(g) pressures required for Reactions 4, 5, 8, and 9 to occur can also drive the following reaction with the CO_2(g) in the combustion environment

$$2MOH(g) + CO_2(g) \rightleftarrows M_2CO_3 + H_2O(g) \quad [10]$$

The partial pressures of all the gaseous species in Reaction 10 are fixed by the temperature and respective compositions of the input fuel/oxidizer ratio and the glass system being melted. Also, in the burning of natural gas by the reaction

$$CH_4(g) + 2\ O_2(g) \rightleftarrows CO_2(g) + 2H_2O(g) \quad [11]$$

it is seen that the H_2O:CO_2 ratio is 2:1, independent of whether the source of oxygen is air or pure oxygen. Thus, the MOH(g) partial pressure in the furnace atmosphere is the variable that determines if Reaction 10 is thermodynamically favorable. Whether or not the alkali carbonate condensed phase can form is determined by the equilibrium constant of Reaction 10, its competition with Reactions 4, 5, 8, and 9 and the partial pressures in the furnace atmosphere. Note, however, that the temperatures required for carbonate formation to occur (<1380 K) are not likely to be encountered by refractories in glass-melting furnaces. Thus, the potential for carbonate formation, while required for a complete thermodynamic treatment, should have no significant impact on alumina corrosion.

Equilibrium predictions of alumina corrosion regimes.—The conditions in glass-melting furnace atmospheres that could lead to corrosion of α- or β-alumina refractories can be determined by performing fixed-temperature equilibrium calculations, using input compositions and a range of temperatures representative of the furnace combustion atmosphere (Table I). Selected results from such calculations for the α-alumina/β-alumina two-phase regions of the Na_2O-Al_2O_3 and K_2O-Al_2O_3 systems are shown in Fig. 3a and b, which display the partial pressures of MOH(g) and M(g) (p_{MOH} and p_M). These are the partial pressures that exist when the gas is in equilibrium with a condensed mixture containing both α- and β-alumina phases. Similar plots are given in Fig. 4a and b for the β-alumina/M_2O-rich phase.

Several general observations for both the sodium and potassium systems can be made from the results in Fig. 3 and 4. First, in their α-alumina/β-alumina two-phase regions (Fig. 3a and b), the partial pressure of MOH(g) always exceeds that of M(g) by a substantial factor under all conditions, confirming that MOH(g) is indeed the equilibrium species that should be of concern in corrosion. Second, the predicted equilibrium MOH(g) partial pressures are always about a factor of two higher in oxy-fired furnace atmospheres than those predicted for air-fired furnaces, which, as discussed previously,[3] is simply a result of the differences in H_2O(g) partial pressures in these two atmospheres (for example, at 1873 K oxy-fired $p_{H_2O} = 0.654$ bar and air-fired $p_{H_2O} = 0.177$ bar). From Reaction 1 or 2, it is seen that the gaseous ratio

$$MOH_{oxy}/MOH_{air} = (H_2O_{oxy}/H_2O_{air})^{1/2} = (0.654/0.177)^{1/2} = 1.92 \quad [12]$$

Finally, Fig. 3a and b show that the concentration of both MOH and M gaseous species increases continuously with temperature up to at least 2100 K. This is quite different from the situation that exists in the M_2O-SiO_2 equilibria, in which there is a maximum in these concentrations at ~1873 K in the Na_2O-SiO_2 system,[3,24] and ~1800 K for the K_2O-SiO_2 system.[3] These temperature maxima are a result of the changing composition of the liquid corrosion product in equilibrium with crystalline SiO_2, which decreases in M_2O concentration with increasing temperature until no M_2O is present in the liquid at the melting point of SiO_2 (cristobalite). As is seen below, the fact that p_{MOH} and p_M increase continuously to very high tem-

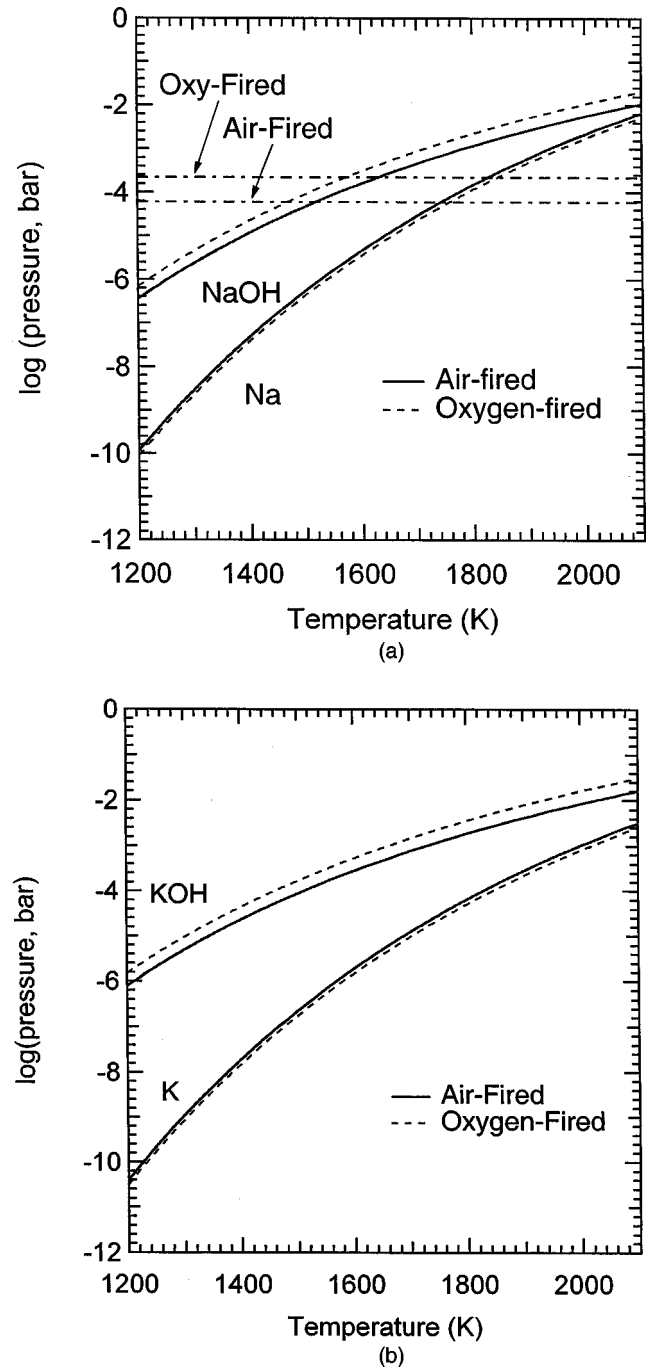

Figure 3. (a) NaOH(g) (upper curves) and Na(g) (lower curves) partial pressures in equilibrium with the α-alumina/β-alumina two-phase region as a function of temperature. The horizontal lines correspond to the example cases for air-fired [50 ppm, $\log P(\text{bar}) = -4.30$] and oxy-fired [200 ppm, $\log P(\text{bar}) = -3.70$] furnaces. (b) KOH(g) and K(g) partial pressures in equilibrium with the α-alumina/β-alumina two-phase region as a function of temperature.

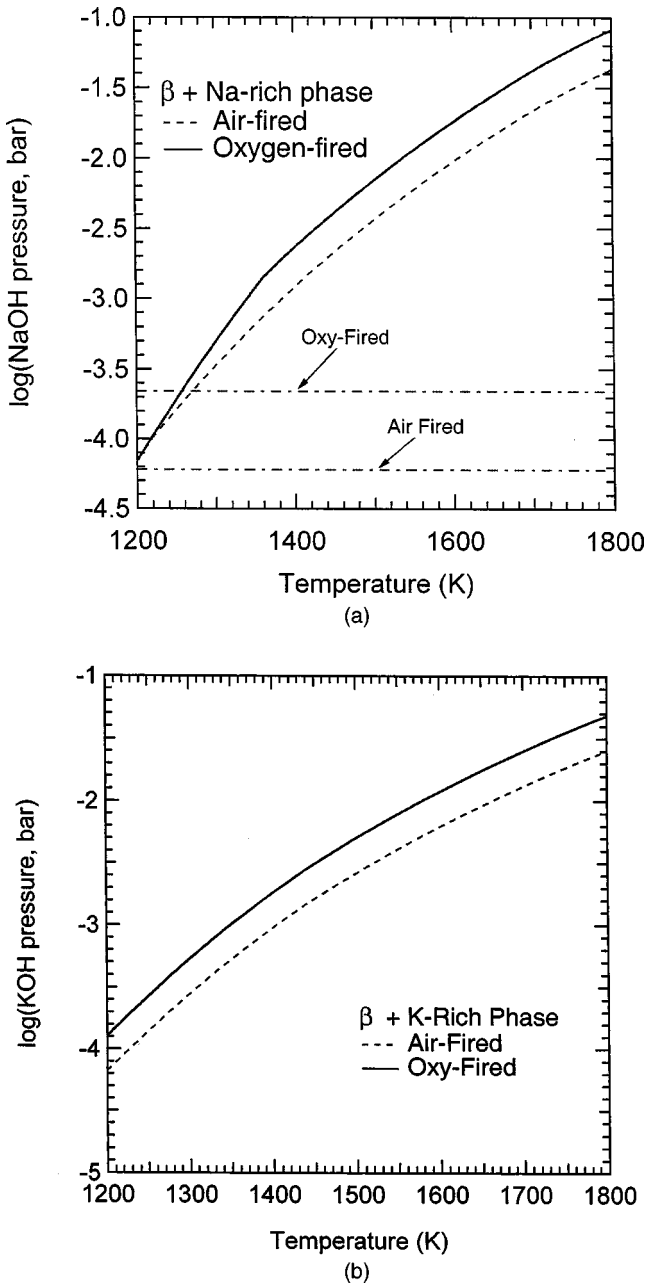

Figure 4. (a) NaOH(g) partial pressures in equilibrium with the β-alumina/Na-rich phase two-phase system as a function of temperature. See text for further description of Na-containing phases as a function of temperature. The horizontal lines correspond to p_{NaOH} example cases for air-fired [50 ppm, $\log P(\text{bar}) = -4.30$] and oxy-fired [200 ppm, $\log P(\text{bar}) = -3.70$] furnaces. (b) KOH(g) partial pressures in equilibrium with the β-alumina/K-rich phase two-phase system as a function of temperature. See text for further description of K-containing phases as a function of temperature.

peratures in the alumina systems has consequences for the corrosion behavior of alumina refractories. Note that the points where the NaOH vapor-pressure curves intersect the horizontal lines in Fig. 3a and 4a (representing values of p_{NaOH} in the combustion atmosphere) indicate the lowest temperature at which the equilibrium vapor pressure exceeds that in the furnace. This leads to the concept of a critical temperature (see below), above which no corrosion can occur. Thus, the predicted equilibrium NaOH(g) concentrations in these figures represent a lower limit for furnace concentrations that can result in corrosion.

Figures 3a and b can be used to identify regions of chemical stability when alumina is exposed to combustion environments reprentative of glass furnaces. In the case of NaOH(g), Fig. 3a indicates that α-alumina should be stable in air-fired furnaces at $T > 1504$ K and in oxy-fired furnaces at $T > 1564$ K, since their respective equilibrium p_{NaOH} for the α-β two-phase system is higher than that found in air- (~50 ppm, or 5×10^{-5} bar) and oxy-fired (~200 ppm, or 2×10^{-4} bar) furnace atmospheres. For similar KOH(g) concentrations in a furnace atmosphere, α-alumina should also be stable at temperatures (Fig. 3b) $T > 1458$ K for air-fired furnaces and $T > 1515$ K for oxy-fired furnaces.

In contrast, ceramics containing sodium β-alumina should decompose to α-alumina and NaOH(g) at $T > 1504$ K (air-fired) and $T > 1564$ K (oxy-fired), since the equilibrium p_{NaOH} exceeds that in the furnace; this phenomenon has been observed.[4] Ceramics containing potassium β-alumina could decompose to α-alumina and KOH(g) when the equilibrium p_{KOH} exceeds the values in the furnace; for furnace KOH(g) pressures of ~50 ppm for air-fired and ~200 ppm for oxy-fired, the respective temperatures are $T > 1458$ K (air-fired) and $T > 1515$ K (oxy-fired).

The β-alumina/M_2O-rich-phase equilibrium is somewhat more complex than the α-alumina/β-alumina equilibrium, since the M_2O-rich product phases in equilibrium with β-alumina depend on temperature. With increasing temperature, the possible product phase changes from β″-alumina to $MAlO_2$(s) to liquid. Figures 4a and b show the p_{MOH} results for two-phase systems when MOH(g) reacts with β-alumina. The nature of these products is indicated by the possible chemical reactions discussed in the previous section. The M_2O-rich product phase in equilibrium with β-alumina in the Na_2O-Al_2O_3 system is Na_2CO_3(s) $T < 1220$ K (air-fired) or $T < \sim 1380$ K (oxy-fired). The difference in these two temperatures is the result of the difference in the assumed p_{NaOH} in the respective combustion atmospheres for air-fired and oxy-fired systems (50 ppm *vs.* 200 ppm p_{NaOH}). At higher temperatures up to 1716 K (1443°C, the β″ peritectoid temperature), β″-alumina forms rather than Na_2CO_3. At even higher temperatures, up to 1857 K (1584°C, the eutectic temperature), β″-alumina is unstable and $NaAlO_2$ forms. Finally, at temperatures between 1857 and 2158 K (1584-1885°C), a sodium-rich (compared to β-alumina) liquid phase forms in equilibrium with β-alumina. As is shown in Fig. 4a for all temperatures> 1260 K the NaOH(g) pressures required to produce these sodium-rich products are much higher than those present in a glass-melting furnace, so such products are not predicted to form under these conditions.

The M_2O-rich product phases in equilibrium with β-alumina in the K_2O-Al_2O_3 system do not include K_2CO_3(s) for the temperatures > 1200 depicted in Fig. 4b. At temperatures above 1200 K, potassium β″-alumina forms rather than K_2CO_3 up to 1435 K (1162°C, the β″ peritectoid temperature) in both air- and oxy-fired environments. At higher temperatures up to 2185 K (1912°C, the eutectic temperature), potassium β″-alumina is unstable and $KAlO_2$ forms. Finally, at temperatures between 2185 and 2262 K (1912-1989°C), a potassium-containing liquid phase forms in equilibrium with β-alumina. As is shown in Fig. 4b for all temperatures > 1260, the KOH(g) pressures required to produce these potassium-rich products are >200 ppm [$\log P(\text{bar}) > -3.70$], the value estimated for p_{NaOH} in oxy-fired glass-melting furnaces. Thus, if KOH(g) levels are comparable to those of NaOH(g), K_2O-rich corrosion products are not predicted to form in these furnace environments.

Figure 4a indicates that the NaOH(g) concentration in equilibrium with the β-alumina/Na-rich product (liquid, $NaAlO_2$, or β″-alumina) two-phase region is much higher than that in equilibrium with the α-β alumina two-phase region (by a factor of 36 at 1800 K for both air- and oxy-fired conditions; at 1200 K, a factor of 200 for air-fired, and 102 for oxy-fired atmospheres). The difference

between the p_{NaOH} ratios at 1200 K for air-fired and oxy-fired conditions is due to the reduction in p_{NaOH} at low temperatures caused by Na_2CO_3 formation in the oxy-fired conditions.

Figure 4a also shows that the equilibrium p_{NaOH} is always higher than typical furnace concentrations for $T > 1250$ K (oxy-fired) and $T > 1200$ K (air-fired), as indicated by the horizontal lines in the figure. Thus, the conversion of β-alumina to β″-alumina or any other Na-rich product phase by NaOH(g) is not thermodynamically feasible, and Reactions 4, 5, and 10 should not occur in typical glass melting furnaces. Similarly, Fig. 4b indicates that the KOH(g) concentration in equilibrium with the β-alumina/K-rich product two-phase system is significantly higher than that in equilibrium with the α-β alumina two-phase system (ranging from a factor of 13 at 1800 K to a factor of 85 at 1200 K for both air- and oxy-fired conditions). Although to our knowledge no KOH(g) furnace concentrations have been reported, Fig. 4b indicates that the equilibrium p_{KOH} is always higher than furnace concentrations of 200 ppm for $T > 1240$ K (oxy-fired), and of 50 ppm for $T > 1200$ K (air-fired). Thus, the conversion of β-alumina to β″-alumina or any other K-rich product phase by KOH(g) is probably not thermodynamically feasible either [again assuming that KOH(g) concentrations are comparable to those of NaOH(g)], and thus Reactions 8, 9, and 10 should not occur in glass melting furnaces.

A final important observation is that M_2O-containing liquid alumina phases are not thermodynamically favored under typical furnace operating conditions, as they are when silica is used. Although the phase diagram for the Na_2O-Al_2O_3 system (Fig. 1a) indicates the possibility of a liquid phase in equilibrium with β-alumina above 1857 K (1584°C), the values of p_{NaOH} in equilibrium with that two-phase region are always much higher than typically observed under either air- or oxy-fired cases, so that one can safely conclude that these liquids will never form.

The data in Fig. 3a and b can be replotted to show temperature as a function of MOH partial pressure to define regions in which corrosion is thermodynamically favored to occur (Fig. 5a and b). In general, corrosion occurs (*i.e.*, α- is converted to β-alumina) in the region of conditions below each curve. For example, if the p_{NaOH} in the combustion atmosphere is higher than that in equilibrium with α- and β-alumina, the boundary line in Fig. 5a, then corrosion can occur. The curves in Fig. 5a and b thus define a critical temperature, ($T_{critical}$) above which corrosion does not occur for a given p_{MOH} in the combustion atmosphere. This concept was introduced previously by Faber and Verheijn[25] and expanded upon by us in subsequent publications.[3,24] Above each curve, corrosion will not occur, since p_{MOH} in the furnace atmosphere is below the equilibrium value for the α-β two-phase region. At NaOH partial pressures representative of oxy-fuel furnaces (~200 ppm), the value of $T_{critical}$ is ~1564 K, Fig. 5a. Under air-fuel conditions, where the NaOH partial pressure is much lower (~50 ppm), $T_{critical}$ is predicted to be ~1504 K. Note that, since our predicted equilibrium p_{NaOH} are expected to be lower limits for the NaOH(g) partial pressures needed to cause corrosion, our predicted values of $T_{critical}$ are actually upper limits for temperatures at which corrosion can occur at a given p_{NaOH} in the furnace atmosphere. Similar arguments can be made for Fig. 5b and KOH partial pressures in the furnace atmosphere.

The fact the curves in Fig. 5 increase continuously with temperature indicates that in the 1200-1800 K temperature range there will always be a temperature above which corrosion will not occur. This contrasts with corrosion of silica refractories, for which, because of a maximum in the p_{MOH} *vs.* $T_{critical}$ curves occurring at ~1800 K, there exist furnace conditions in which corrosion is always thermodynamically favored. A similar maximum also occurs in the M_2O-Al_2O_3 systems, but only at high temperatures where α-alumina can exist in equilibrium with a liquid phase, between 2158 and 2327 K for the sodium system, and between 2257 and 2327 K for the potassium system. Therefore, a maximum in the p_{MOH} *vs.* $T_{critical}$ curves for the alumina systems would never be observed under practical glass-melting conditions.

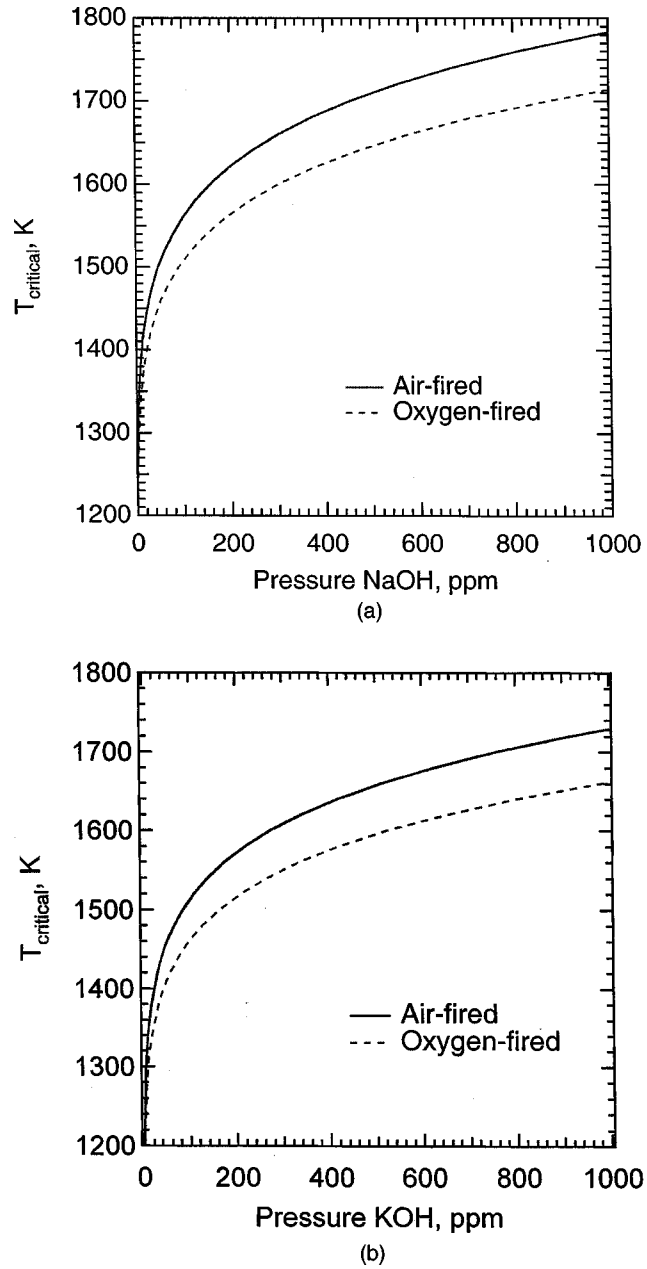

Figure 5. (a) Zones of alumina refractory corrosion by NaOH(g) as defined by $T_{critical}$ (see text) for the α-alumina/β-alumina two-phase region. The NaOH concentrations are given in units of ppm (parts per million at 1 bar) since this is the common measure of most glass manufacturers (we use the conversion of 1 ppm = 1×10^{-6} bar). (b) Zones of alumina refractory corrosion by KOH(g) as defined by $T_{critical}$ (see text) for the α-alumina/β-alumina two-phase region. The KOH concentrations are given in units of ppm (parts per million at 1 bar).

The results presented above suggest that there may be several advantages to using high-purity α-alumina as a crown material. First, $T_{critical}$(oxy) of 1564 K for 200 ppm NaOH(g) in the furnace atmosphere is considerably below the operating temperatures typically used for silica crowns (maximum continuous operating temperatures ~1853-1873 K), indicating that α-alumina should be thermodynamically stable in this temperature regime. Second, replacement of silica with alumina may provide additional flexibility

with regard to burner optimization. Burner placement has been shown to affect crown temperatures; placing burners higher on the furnace wall (which may reduce NaOH and KOH volatilization rates) increases crown temperatures in some locations.[5] Since the temperatures at which alumina either melts or forms liquid corrosion products are much higher than 1873 K (Fig. 1a and b), it can tolerate placement of burners in locations closer to the crown. Finally, the formation of liquid sodium silicates from the corrosion of silica refractories is much more deleterious to the refractory than the formation of β-alumina from the corrosion of α-alumina. The mechanical properties of corroded alumina refractories are evidently sufficient to inhibit structural damage.[4]

Conclusions

The thermodynamic calculations reported here, using newly generated data for sodium- and potassium-containing alumina phases, indicate that alumina is quite stable with respect to corrosion by MOH(g) under the conditions typical of glass-melting furnaces. Unlike silica, liquid-phase alkali aluminates are not stable except at very high temperatures and in equilibrium with extremely high MOH(g) partial pressures, indicating that these liquid products will not form. Thus, problems associated with formation of liquid corrosion products, such as run off of corrosion products into the melt and presumably, unacceptably high corrosion rates (as is the case for silica), should not be a problem for crowns constructed of either α- or β(Na)-alumina used in oxy-fuel melting furnaces. The negative aspect of using alumina refractories instead of silica is that they are heavier, so that glass-melting furnaces require special construction. They are also more expensive than silica, raising the capital costs of such furnaces.

Acknowledgments

The authors are grateful to the following organizations for their financial support of this project: the U.S. Department of Energy (DOE), Office of Industrial Technologies, Glass Industry of the Future Team; American Air Liquide; BOC Gases; PPG Industries, Inc.; Praxair, Inc., Techneglas; Visteon Automotive Systems; and the DOE Environmental Management Science Program funded by the Office of Environmental Management's Office of Science and Technology, and administered jointly with the Office of Energy Research under contract DE-AC05-00OR22725 with UT-Battelle, LLC.

Sandia National Laboratories assisted in meeting the publication costs of this article.

References

1. *Corrosion of Materials by Molten Glass*, G. A. Pecoraro, J. C. Marra, and J. T. Wenzel, Editors, Vol. 78, American Ceramic Society, Westerville, OH (1996).
2. K. T. Jacob, K. Swaminathan, and O. M. Sreedharan, *Electrochim. Acta*, **36**, 791 (1991).
3. M. D. Allendorf and K. E. Spear, *J. Electrochem. Soc.*, **148**, B59 (2001).
4. H. T. Godard, L. H. Kotacska, J. F. Wosinski, S. M. Winder, A. Gupta, K. R. Selkregg, and S. Gould, *Ceram. Eng. Sci. Proc.*, **18**, 181 (1997).
5. K. T. Wu and H. Kobayashi, in *Corrosion of Materials by Molten Glass*, Vol. 78, G. A. Pecoraro, J. C. Marra, and J. T. Wenzel, Editors, p. 205, American Ceramic Society, Westerville, OH (1996).
6. J. A. M. van Hoek, F. J. J. van Loo, and R. Metselaar, *J. Am. Ceram. Soc.*, **75**, 109 (1992) and references therein.
7. G. Dewith, P. J. Vrugt, and A. J. C. Vandeven, *J. Mater. Sci.*, **20**, 1215 (1985).
8. S. K. Sundaram, J. Y. Hsu, and R. F. Speyer, *J. Am. Ceram. Soc.*, **78**, 1940 (1995).
9. S. K. Sundaram, J. Y. Hsu, and R. F. Speyer, *J. Am. Ceram. Soc.*, **77**, 1613 (1994).
10. H. Näfe, *J. Electrochem. Soc.*, **143**, 943 (1996).
11. A. J. Faber and O. S. Verheijen, *Ceram. Eng. Sci. Proc.*, **18**, 109 (1997).
12. G. Eriksson, P. Wu, and A. D. Pelton, *CALPHAD: Comput. Coupling Phase Diagrams Thermochem.*, **17**, 189 (1993).
13. R. S. Roth, *Adv. Chem.*, **186**, 391 (1980).
14. R. V. Kumar and D. A. R. Kay, *Metall. Mater. Trans. B*, **16**, 295 (1985).
15. A. Petric and C. Chatillon, in *High Temperature Materials Chemistry IX*, K. E. Spear, Editor, PV 97-39, p. 718, The Electrochemical Society Proceedings Series, Pennington, NJ (1997).
16. M. Barsoum, *J. Mater. Sci.*, **25**, 4393 (1990).
17. G. M. Kale and K. T. Jacob, *Metall. Mater. Trans. B*, **20**, 687 (1989).
18. M. Itoh and Z. Kozuka, *J. Am. Ceram. Soc.*, **71**, C36 (1988).
19. G. Eriksson and K. Hack, *SGTE Pure Substance Database*, 1996 Version, produced by the Scientific Group Thermodata Europe and obtained through GTT Technologies, Herzogonrath, Germany (1996).
20. M. J. Chase Jr., *J. Phys. Chem. Ref. Data*, Monograph 9, 1, NIST-JANAF Thermodynamic Tables, 4th ed. (1998).
21. *ChemSage™ 4.1*, GTT Technologies, Herzogonrath, Germany (1998).
22. K. E. Spear, T. M. Besmann, and E. C. Beahm, *MRS Bull.*, **24**, 37 (1999).
23. *Phase Diagrams for Ceramists*, Vol. 1-12, The American Ceramic Society, Westerville, OH (1964-1996).
24. K. E. Spear and M. D. Allendorf, in *High Temperature Corrosion and Materials Chemistry, The Per Kofstad Memorial Symposium*, M. McMallan, E. Opila, T. Manayama, and T. Narita, Editors, PV 99-38, p. 439, The Electrochemical Society Proceedings Series, Pennington, NJ (1999).
25. A. J. Faber and I. O. S. Verheijen, Report NCNG-Project: Reduction of Refractory Corrosion-Phase 1, TNO Institute of Applied Physics (1996).
26. S. G. Buckley, P. M. Walsh, D. W. Hahn, and R. J. Gallagher, *Ceram. Eng. Sci. Proc.*, **21**, 183 (2000).